Heritage Science

RESEARCH

Open Access

Acquisition strategies for in-situ hyperspectral imaging of stained-glass windows: case studies from the Swiss National Museum

Agnese Babini[1*], Tiziana Lombardo[2], Katharina Schmidt-Ott[2], Sony George[1] and Jon Yngve Hardeberg[1]

Abstract

Over the last decade, hyperspectral imaging has become a popular technique for the non-invasive identification and mapping of painting materials in many typologies of artworks, thanks to the possibility of obtaining spectral information over the spatial region. A few attempts have also been made on stained-glass windows to identify the chromophore elements responsible for glass color. Hyperspectral imaging of stained glass can be complex; in most cases, stained-glass windows are an integral part of buildings, and sunlight represents the natural light source for illuminating these artifacts. While it may be considered an advantage, sunlight is not homogeneous throughout the day, and different weather conditions can affect the quality of the hyperspectral images. In addition, the presence of buildings and vegetation in the background could also modify the colors of the stained-glass windows and consequently alter the characteristic peaks of the chromophores in the spectra. This work aims to solve some of these issues and proposes different strategies to improve the results obtainable in situ. The methodology was tested on stained-glass panels displayed in the windows of the Swiss National Museum. Stained-glass panels located in windows of an internal wall were also analyzed, developing a lighting setup to account for the lack of natural light. Hyperspectral images of the selected stained glass were acquired multiple times, choosing different transmittance references for the preprocessing and exposure time to evaluate differences in the collected spectral images. The use of a diffuser sheet to mitigate the effect of external factors was also tested on some panels exposed to sunlight. Results from representative case studies will be presented to discuss the feasibility and limitations of in-situ hyperspectral imaging applications on stained glass and provide some general recommendations to consider during the acquisitions.

Keywords Stained-glass, Hyperspectral imaging , Transmittance, In-situ measurement

Introduction

Since its first application in the cultural heritage field, over the years, hyperspectral imaging (HSI) has become a versatile technique for the non-invasive investigation of works of art [1]. This technique is based on the acquisition of many images finely sampled across a portion of the electromagnetic spectrum; as a result, a three-dimensional image is created (often referred to as a datacube) consisting of two spatial and one spectral dimension. In this way, a full spectrum can be obtained in each pixel of the image, providing information on the materials used

*Correspondence:
Agnese Babini
agnesebabini3@gmail.com
[1] Department of Computer Science, NTNU - Norwegian University of Science and Technology, Teknologivegen 22, 2815 Gjøvik, Norway
[2] Collection Centre, Swiss National Museum, Lindenmoosstrasse 1, 8910 Affoltern Am Albis, Switzerland

as well as their distribution across the artwork under study [2]. Various HSI systems have been developed to analyze and document paintings on different supports, manuscripts, and photographic materials [1–9]. A few papers have also been published recently regarding the application of HSI on stained-glass windows to identify the chromophore elements responsible for glass color [10–15]. However, research on this topic is still limited; imaging stained glass can be complex, and many factors must be considered. If the stained glass panels are removed from their original location (e.g., for restoration treatments), or in the case of separately stored panels, it is possible to use acquisition systems based on standard transmittance geometry and stable light sources, such as halogen lamps [13, 15]. Thanks to these characteristics, such setups allow for comparable results to UV–VIS-IR spectroscopy, a widely used technique to analyze historical and archaeological glass [14].

However, in most cases, stained-glass windows are an integral part of buildings, and due to their transparency, solar radiation represents the natural light source for the illumination of these artifacts. Palomar et al. [12], were the first to explore the potential of this technique to identify the chromophore elements of an Art Nouveau stained-glass window, exploiting solar radiation as a light source. The work showed promising results, and the authors were able to distinguish and map glass with the same color and composition but different transparency, despite the changing light conditions. Nonetheless, the paper stressed how the vegetation in the background could affect the spectra of light-colored glass and the difficulties in identifying the chromophores in the spectra of dark-colored glass. Funatomi et al. [10], explored the possibility of reconstructing a spectral datacube from raster scanning fiber optic to solve the issue of illumination variation during the acquisition. However, the proposed methodology is still in the experimental stage and is not publicly available.

The aim of this research is to propose acquisition strategies to tackle those challenges and improve results from *in-situ* hyperspectral imaging of stained-glass windows using a commercially available camera. The proposed methodology was tested on eight stained-glass panels displayed in windows at the Swiss National Museum, chosen after discussion with the museum conservators considering various factors related to the environment and the artwork characteristics. In order to evaluate the quality of the HSI datacubes obtained in different contexts, all the case studies were captured multiple times, selecting various transmittance references for the preprocessing. Some panels exposed to sunlight were captured before and after placing a diffusing sheet behind the windows and, in a few cases, acquired at different moments of the day. To the best of the authors' knowledge, this is the first time HSI has been applied to analyze stained glass in such a systematic way.

Stained-glass panels located in windows of an internal wall were also chosen; since they are not directly exposed to the sun, the analysis of these case studies allowed studying a different solution to make the acquisition possible. A lighting setup consisting of a photography light diffuser and a halogen lamp was developed and tested for the purpose.

Results from five representative case studies, four exposed to natural sunlight and one from the internal wall, will be presented to compare the different acquisition scenarios (natural vs. artificial illumination) and discuss the proposed methodology's contributions and limitations.

Experimental

Case studies

Eight stained-glass panels were chosen for the experiments; the selection was based on the panels' location, sun exposure, homogeneity of the background behind the windows, and artistic attributes. The influence of these parameters will be discussed in detail in "Results" section. Six of those panels are displayed within the external windows of the Swiss National Museum, while two are located in windows of an internal wall. After a preliminary data interpretation of all eight case studies, five of them were chosen as the most representative to discuss the main findings of the research and answer specific research questions. Technical information, the number of acquisitions performed, and the research questions addressed by each case study are summarized in Table 1.

Regarding the discarded case studies, one of them was made of very dark-colored pieces of glass, and it was impossible to obtain satisfying results. The other two case studies, one exposed to sunlight and one located in the inner window, have very similar palettes to the case studies discussed in this paper. For this reason, it was decided not to include them in the manuscript; however, results from these two panels are available in Additional file 3.

Setup

A portable push-broom hyperspectral camera (Specim IQ, Specim, Spectral Imaging Ltd.) was employed for the experiments. The camera acquires 204 bands between 400 and 1000 nm in visible and near-infrared (VNIR region) and has a spatial sampling of 512 pixels per line. Since the number of imaged lines is fixed to 512, the result is a square image with a resolution of 512×512 pixels. The field of view is $31° \times 31°$. The image's actual resolution depends on the distance the camera was

Table 1 Summary table containing technical information, the number of acquisitions taken, and the research questions for each case study analyzed in the paper

Case studies	Information	Number of acquisitions	Research questions
IN-64.11	Author: Hans Caspar Lang Date: 1609 Dimension: Ø 19,6 cm Location: Lochmannsaal Description: Allianzscheibe. Ornamental rim with scroll-work motifs and putti heads. Content: Alliance coat of arms Hans and Barbara Im Thurn-Peyer. Lion head motif (coat of arms)	13	Effects of background Effects of selection of different areas as reference for Radiometric correction evaluation of differences in acquisitions taken at different times of the day
AG-1177	Author: N/A Date: 1574 Dimension: Ø 21,5 cm Location: Lochmannsaal Description: Allianzscheibe. The two coats of arms stand between two strong columns in front of a colorless background. Content: Alliance coat of arms of Marx and Margaretha Escher-Blarer von Wartensee	12	Effects of background and vegetation Effects of selection of different areas as reference for radiometric correction
LM-8368	Author: N/A Date: 1599 Dimension: 31,8 × 22,2 × 0,6 cm Location: Rosemburgsaal Description: Bauernscheibe. Man as halberdier in a blue robe, his wife in a red skirt. Content: Married couple Jos Abderhalden. Dairy farming (upper image)	4	Effects of background and vegetation Effects of selection of different areas as reference for radiometric correction
LM-749	Author: N/A Date: 1627 Dimension: 30.2 × 19.6 cm Location: Seidenhof (internal wall) Description: Wappenscheibe. Queen of Sheba at King Solomon, giving him the flower riddle. Content: personal coat of arms Christoph Werdmüller	8	Development of a setup for stained glass not exposed to sunlight Material identification and distinction
LM-660.1	Author: N/A Date: 1567 Provenance: Entlebuch Dimension: 46.1 × 33.5 × 0.7 cm Location: Rosenburgsaal Description: Bannerträgerscheibe from Entlebuch. Content: horseman	6	Effects of background and vegetation Material identification and distinction

positioned during the measurement. Details are given in Additional file 1: Tables s1–s5).

Further technical details regarding the camera are described in [16, 17]. Compared to other line scanner cameras, which are relatively heavy and must be mounted on translating or rotating stages, this camera has the advantage of being smaller, lighter, and more compact and offers easy mobility within the museum's spaces. The museum environment was an important aspect to consider since the rooms have historical walls and floors, and fragile artworks are exposed in the proximity of the area required for the scanning. For this reason, portable cameras like the Specim IQ were preferred for the experiment.

The camera was mounted on a tripod that could reach a maximum height of around 220 cm (Fig. 1). A table was used in specific cases to achieve an optimal height. Since the camera offers the flexibility to adjust focus distance, it was possible to place it in a way that allowed acquiring the entire panels in a single acquisition. Sunlight was used as the light source for all the panels except for LM-794, which is installed in the window of the internal wall. In this case, a temporary transmittance setup was developed using a photography light diffuser and a halogen lamp (Fig. 2).

All the configurations were previously evaluated in the laboratory using mock-up glass. Those tests were crucial to optimize the acquisition process since the time allocated for the imaging campaign was constrained by the museum's opening hours, and only 2 days were available on site.

In order to evaluate the best imaging conditions and parameters, the panels were acquired multiple times. With regard to the panels exposed to sunlight, a novel

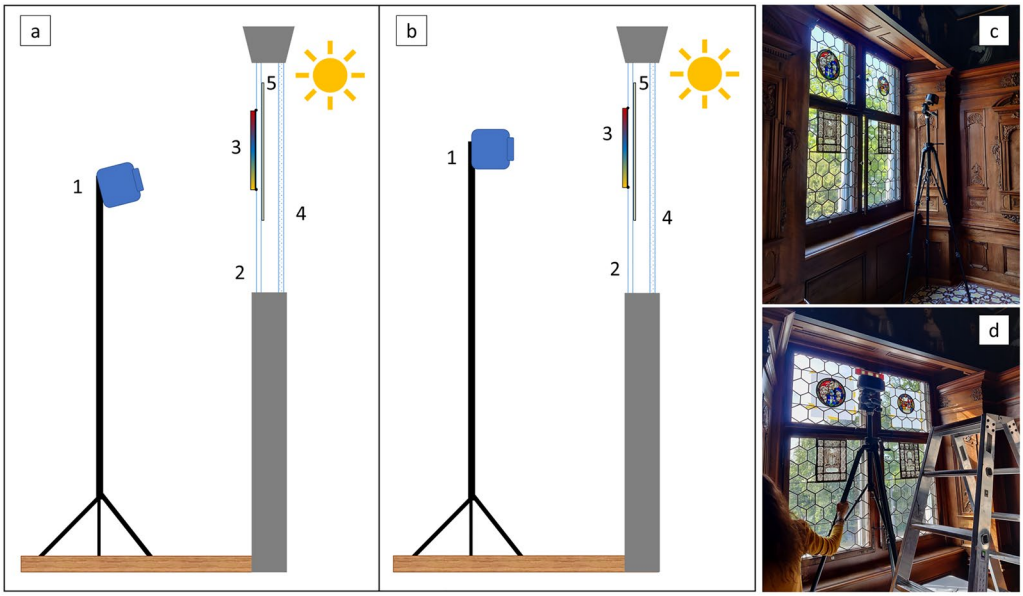

Fig. 1 **a**, **b** Schematics of the set-up for the stained-glass panels exposed to sunlight: 1) hyperspectral camera; 2) historical glass; 3) stained-glass panel; 4) modern glass. 5) Baking paper (diffusing sheet). **c**, **d** Pictures of the setup in use during the campaign

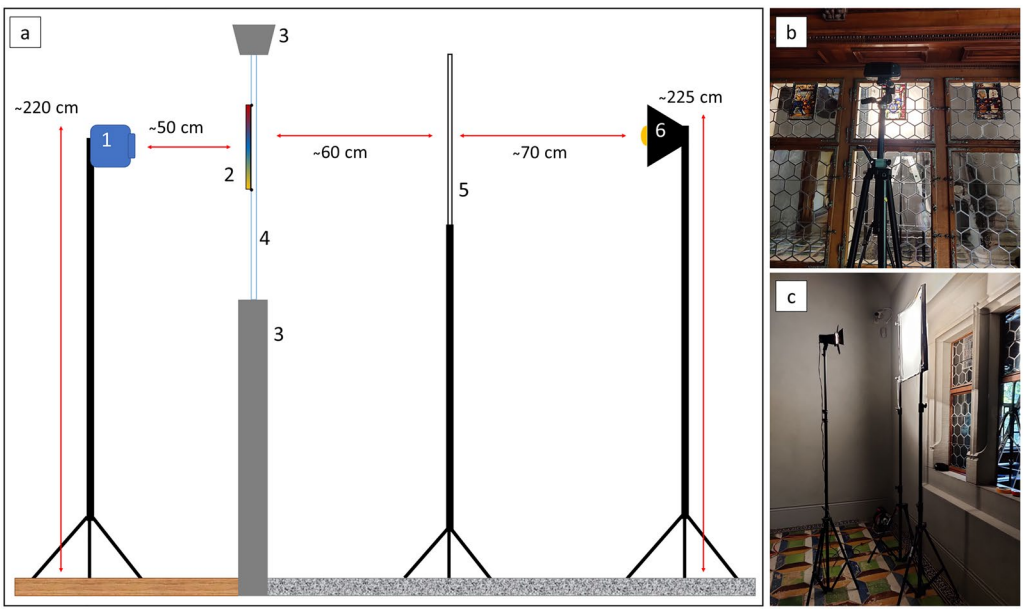

Fig. 2 **a**, **b** Schematics of the set-up for the stained-glass panels exhibited in the inner wall: 1) hyperspectral camera; 2) stained-glass panel; 3) wall; 4) historical glass; 5) diffusing fabric; 6) light source. **c**, **d** Pictures of the setup in use during the campaign

approach was tested to limit the interference of the environment behind the windows on the color of the glass. This approach involves placing a baking paper sheet behind the stained glass to be analyzed. The baking paper represented an affordable yet efficient solution to diffuse the light since it is thin, lightweight, and easy to attach to glass surfaces using simple masking tape. This method could be implemented because the stained-glass panels are encased in historical windows, which were moved and integrated into the museum spaces together with the stained-glass panels. These historical windows are, in turn, protected by additional modern windows (Fig. 3).

After discussing with the museum conservators, it was possible to open the historical windows partially and

Fig. 3 Examples from the acquisitions of case studies IN-64.11; the diffusing sheet is placed on the glazing (historical window) behind the stained glass panel, so that it is not in touch with the artwork. In case of IN-64.11 the historical window was kept open to avoid having the tower (on the left side) within the field of view during the acquisition. For the other case studies the historical windows were closed after placing the diffusing sheet

attach the diffusing sheet behind the stained-glass panel (Fig. 3).

Figure 4 shows the rooms' orientation and the stained-glass panels' location within the room. Additional file 1: Tables s1–s5 reports the conditions and parameters of the acquisitions of the five stained glass panels discussed in this paper. Figures showing the sun's position during the acquisitions of IN-64.11, AG-1177, and LM-8368 are available in Additional file 1: Figs. s1–s3).

Image preprocessing

The image preprocessing is performed by the camera software directly during the acquisition. The default recording mode of the camera was used for almost all the recordings; in this mode, there are two options to perform the radiometric correction from raw data to reflectance (transmittance in this case). The first option ("simultaneous mode") is to select an area representing the white reference from the scene itself. The stored signal is then used to process the image before saving it (Fig. 5). The second option ("custom mode") allows the user to record and store the entire background as a reference. This reference can then be used for all the subsequent measurements. Since it was not possible to completely open the windows to capture the background, "simultaneous mode" was used for almost all the acquisitions. An attempt to use custom mode was performed only on case study LM-660.1 since it is located in a window that can be fully opened, but it was decided that presenting the results from this mode was beyond the scope of this paper. A detailed workflow of the camera acquisition process is described by Behmann et al. [16].

Once the acquisition is finished, the obtained output is a dataset made of separate folders containing the raw datacube (together with the dark current and the white reference data), the processed datacube, and the metadata file. The processed datacubes were analyzed through the Fiji implementation of the open-access software ImageJ [18].

Results

Panels exposed to solar radiation

In order to understand the main contribution of in situ hyperspectral imaging of stained-glass windows, it is important first to address the most common challenges that must be taken into consideration during the imaging process. With regards to the stained-glass windows exposed to sunlight, these challenges can be distinguished into three groups:

- Camera-related: transmittance reference acquisition, storage, and use during the radiometric correction process.
- Imaging environment-related: changes in lighting conditions while utilizing solar radiation as the source of light due to the variation of sun position; changes in atmospheric condition; the presence of buildings, vegetation, or other such obstacles behind the stained glass; noise from atmospheric water (H_2O) absorption band in NIR region (925–970 nm) [16].
- Object-related: transparency, translucency, and thickness of the colored glass; possibility to select a suitable transmittance reference (transparent glass) within the field of view; chemical composition of the reference transparent glass.

Despite this categorization, it is important to stress that those challenges are closely intertwined and should not be considered separately. In this section, results from the selected case studies will be shown to provide practical examples of the effects of these factors and the solutions adopted to limit them.

Reference selection: consequences of a non-homogeneous background and light variation

The selection of a suitable reference for radiometric calibration is a fundamental aspect to take into consideration

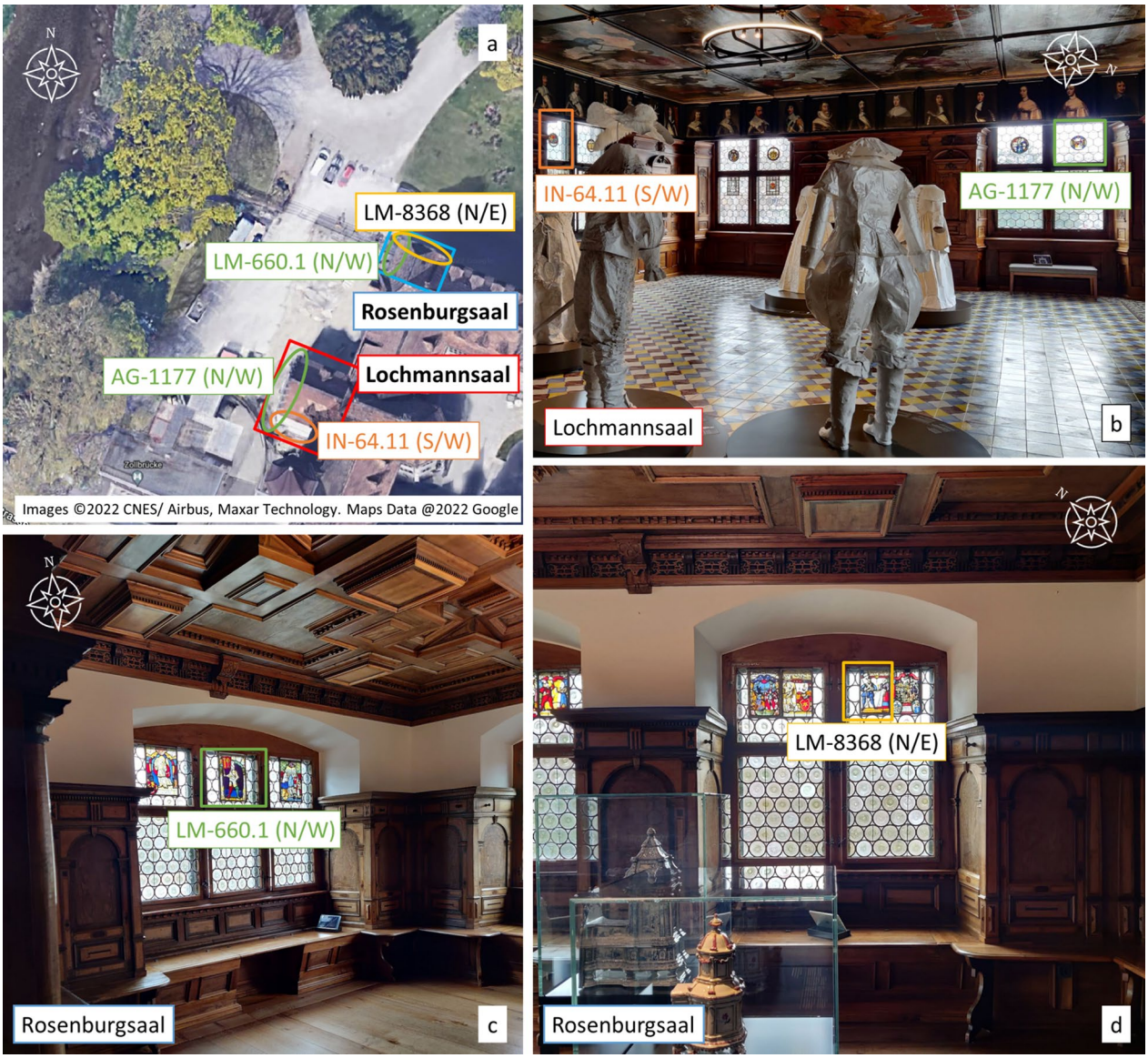

Fig. 4 **a** Aerial view of the Swiss National Museum, showing the overall orientation of the rooms and the selected panels. **b**–**d** Figures showing the specific location of each panel within the room where they are exhibited

during HSI acquisition and processing. The best option would be to acquire an image of the background without the stained glass, representing the light distribution of the entire field of view, ideally as homogeneous as possible. In most in-situ scenarios, however, the stained glass occupies the whole window space, and often the reference must be selected from transparent pieces within the stained glass itself.

Referring to the case studies presented in this paper, two distinct scenarios can be noticed. In the first case, the panels are installed in a historical window consisting of flat hexagonal glass panes (Fig. 6).

In this case, the reference can be picked in one of the panes closer to the panel, and since they are relatively large, the signal obtained can be considered representative of at least a portion of the stained glass. In the second scenario (see section "Stained glass within crown-glass windows", Fig. 12a), the stained-glass panels are located within a crown glass window; in this case, only the tiny glass triangles between the crown glass can be used for image processing since they are flat and uncolored. The availability of such a small area as a reference represents a disadvantage, as it can be considered representative of only a minimal part of the field of view. In the following

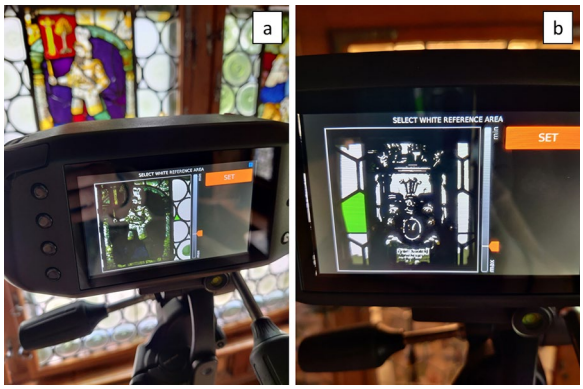

Fig. 5 Reference region selection step during the acquisition process of the case study LM-660.1 (**a**) and LM-789 (**b**). The camera shows areas with the same intensity (in white) from where the most suitable reference can be chosen (in green)

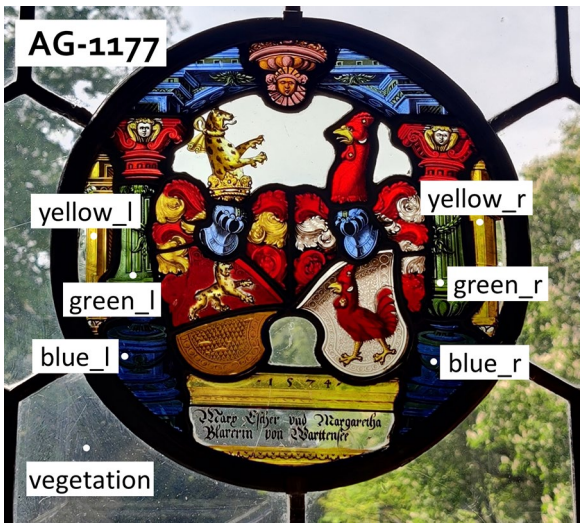

Fig. 6 Close-up picture of case-study AG-1177, showing the points selected for the spectra comparison. The vegetation in background is very visible from the transparent glass surrounding the stained-glass

sections, examples from the two scenarios will be shown to demonstrate how these situations affect the quality of the results.

Stained glass within windows with hexagonal panes Figure 6 shows the example of case study AG-1177; the panel is oriented North/West, which means it receives most of the sunlight in the afternoon from the left side. At the moment of the acquisition, the sky was cloudy; in addition, trees can be observed in the background.

The first step to exclude the presence of the trees inside the camera field of view was to tilt the camera to a certain degree (see Table 1s in Additional file 1 for details). Since the tilting angle is relatively small (15° on average), the geometric distortions are negligible and do not affect the data interpretation. Despite this solution, however, it can be noticed that the trees are still visible on the left side in acquisitions #1 and #2 (Fig. 7a and e).

Figure 7b–d and f–h show how the spectra of glass sections with the same color appear entirely different, whether collected from the left or right side of the panel. In fact, it can be noticed that the characteristic peaks of chromophores are covered by the signal of vegetation in all the spectra obtained on the left side. In this case, the possibility of placing a diffusing sheet behind the stained glass, covering the entire field of view, represented a good solution to improve the quality of the spectra taken from the left side, as the peaks associated with the vegetation are eliminated (Fig. 7j–l).

Nonetheless, despite the use of a diffusing sheet, variations of spectra intensity and shape can still occur. Figure 8 shows six acquisitions carried out in different configurations: the first group (acquisitions #4, #6, and #7) was acquired between 4:40 pm and 4:45 pm, with the camera tilted at around 15°. The second group of images (#9, #10, and #12) was recorded between 5:30 and 5.40 pm with the camera facing the panel straight. In addition, for each group, the transparent reference was selected in three different areas: on the right (acquisitions #4 and #9), inside the panel (acquisition #6 and #12), and on the left (acquisition #7 and #10) (Fig. 8).

Figure 9 shows the spectra plots obtained from yellow, green, and blue glass selected on the left and right sides of the panel. For each colored glass, the comparison is also made between the pair of datacubes acquired with the same hexagonal glass pane as reference but taken at different camera inclinations. In most cases, the spectra from the two sides are more comparable, sometimes even overlapping, when taken from the second group of images (orange, red, and yellow lines). Having the camera facing straight may have contributed to improving the results for the second group of datacubes; however, the main reason behind this behavior is most probably related to the sun's position during the acquisitions.

The six acquisitions were made within one hour, from around 4.40 pm to 5.40 pm. Since the panel is exposed North/West and the datacubes were collected in mid-late afternoon, the sunlight hit the stained-glass panel from the left side. It can be noticed from Fig. 8c–f how acquisitions #7 and #10, where the reference was selected on the left side, are less affected by the light changing during the imaging session, as the two images show a similar light distribution. On the other hand, acquisitions #4 and #9 show some differences, especially in the lower part of the image, which appears less illuminated in acquisition #9. This may also explain why the spectra of acquisitions #7

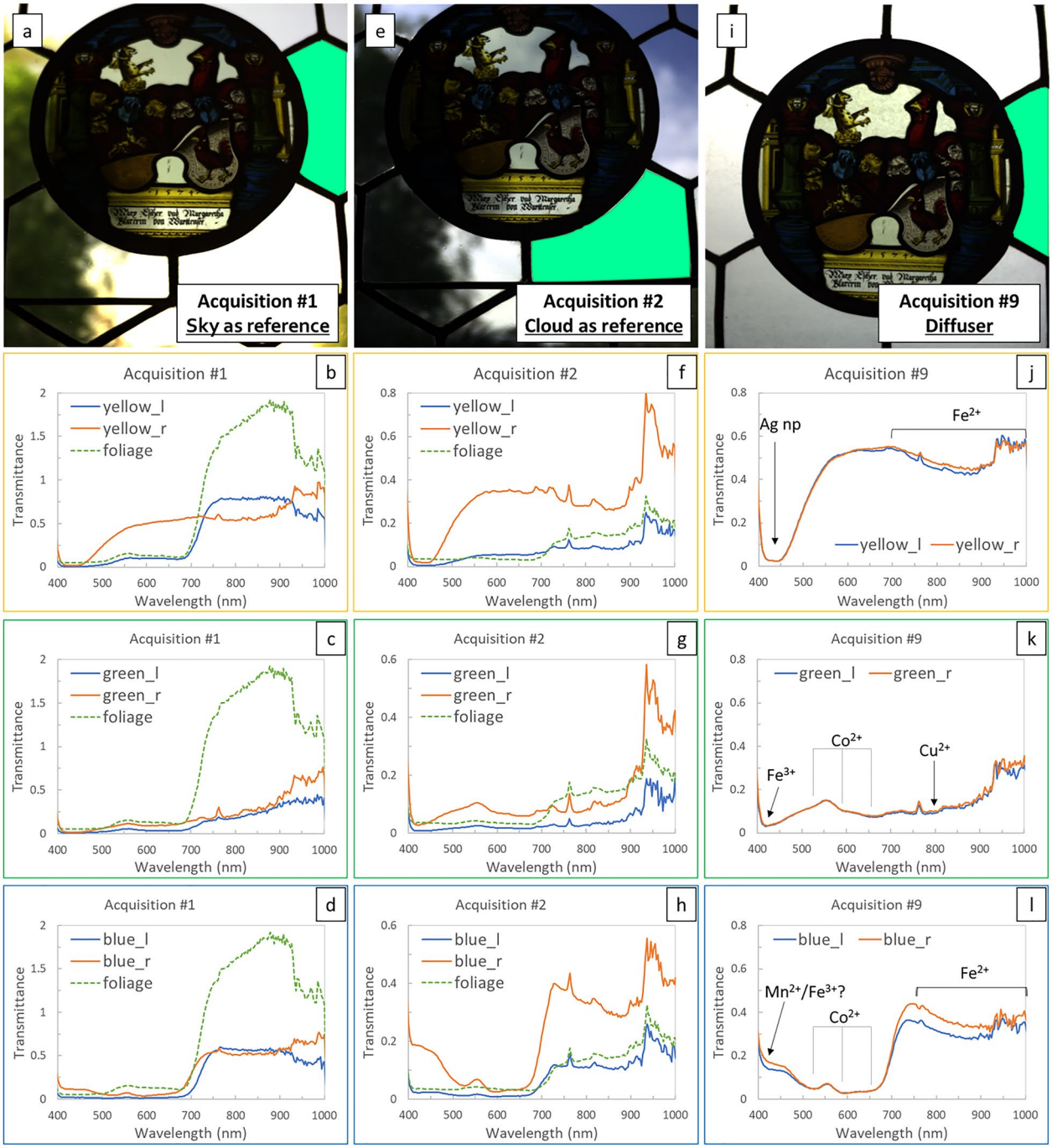

Fig. 7 **a**, **e**, **i** Pictures showing the areas chosen as transmittance reference (in green). **b**–**l**) spectra comparison for the three selected colors (yellow, green, and blue) from acquisition #1 (**b**–**d**), acquisition #2 (**f**–**h**) and acquisition #9 (**j**–**l**). The bands' position of the main chromophores (np = nanoparticles) are indicated with arrows, except for Fe^{2+}. Since the maximum of the Fe^{2+} band falls outside the camera spectral range (1100 nm), and the NIR region is quite noisy, it was preferred to indicate the band width for this chromophore. The peak at 750 nm is an artifact probably due to the sunlight spectrum or interference from the atmosphere. Postfixs in curve labeling: l = left; r = right. Figure 6 shows the points where the spectra were taken

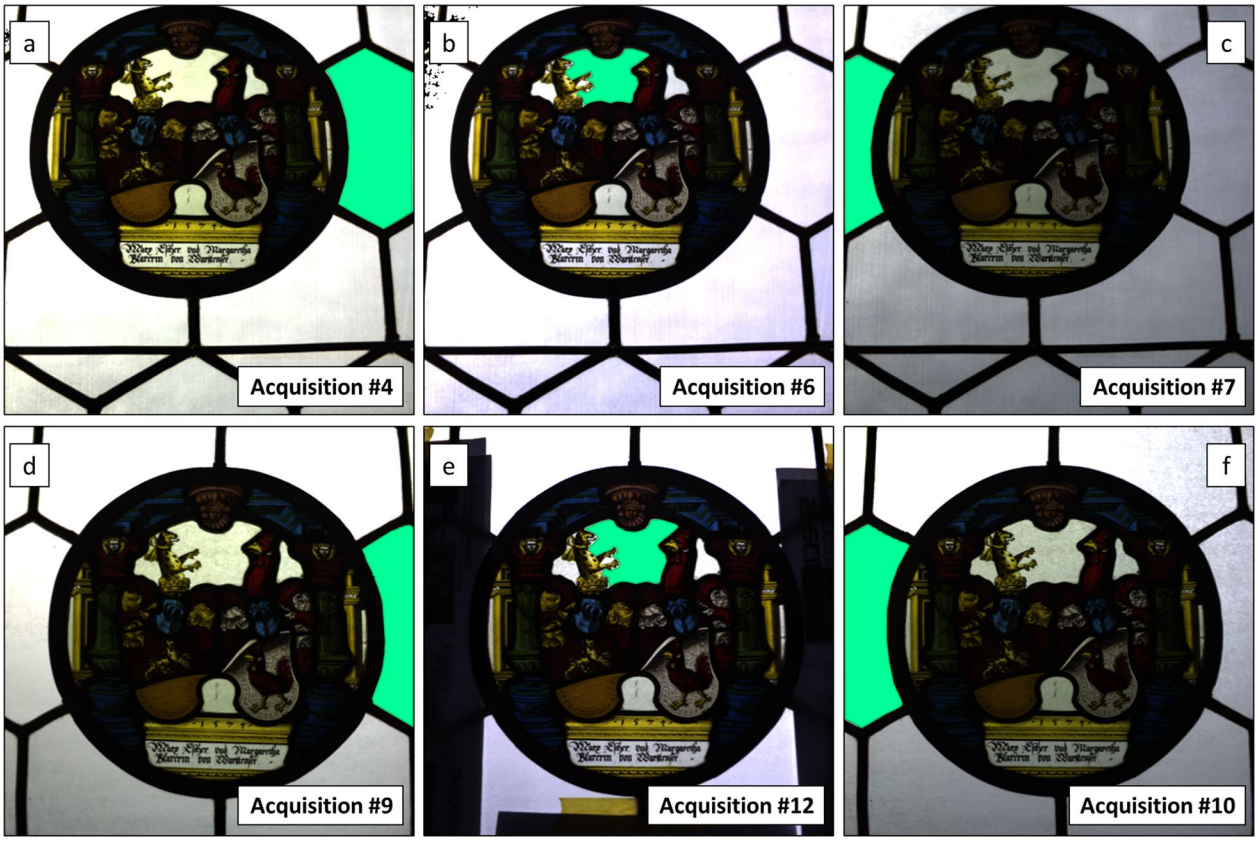

Fig. 8 Pictures showing the areas chosen as transmittance reference (in green) for the acquisitions #4 to #12 of the case study AG-1177. The differences between the pictures in the first row and the ones in the second row are due to the inclination of the camera during the recording of the first set of images. Acquisitions #4 and #9 (**a**, **d**), #6 and #12 (**b**, **e**) and #7 and #10 (**c, f**) were processed using the same glass pane. Some paper sheets were also placed on the sides of the panel during acquisition #12 to decrease the contrast between the dark colored glass and the transparent ones

and #10 are more comparable in terms of intensity than the other two couples of datacubes.

Different spectral shapes are clearly visible, especially in the NIR region for the spectra obtained from the datacubes processed with the transparent glass within the stained glass and those processed with the transparent glass from the historical window. These differences influence the identification of the signature band of ferrous iron (Fe^{2+}), characterized by a broad absorption with a maximum at around 1100 nm [19, 20] (outside of the Specim IQ camera sensitivity), and it is related to the chemical composition of the glass selected as the reference. This aspect will be explained further in the "Discussion" section.

Another example of the influence of light variation is given by case study IN-64.11 (Fig. 10); this panel is oriented South/West and, differently from AG-1177, has a clear background. A tower outside can be seen on the left side, but the possibility of partially opening the window (Fig. 3) allowed for excluding its presence in the image during the HSI acquisition.

The HSI of this stained glass was performed at two specific moments of the day. The first set of images (acquisitions #7 and #9) was recorded in the late morning (11.20–11.25 am); the sun was high in the sky but covered by the tower outside on the left. The second set was recorded mid-afternoon, between 15.46 and 16.17 (acquisition #10 and #13), with the sun well visible on the right side of the field of view.

As for the case study AG-1177, three pairs of colored glass present specularly on the left and right sides were chosen for comparison. It can be noticed how the spectra taken from the datacubes recorded in the morning (#7 and #9) are separated into two distinct groups. The first group (Fig. 11, light-colored lines) represents the spectra taken from the right side of the two datacubes, while the second one (Fig. 11, dark-colored lines) represents the ones taken from the left side. In general, the spectra collected on the right side seem to have a lower intensity

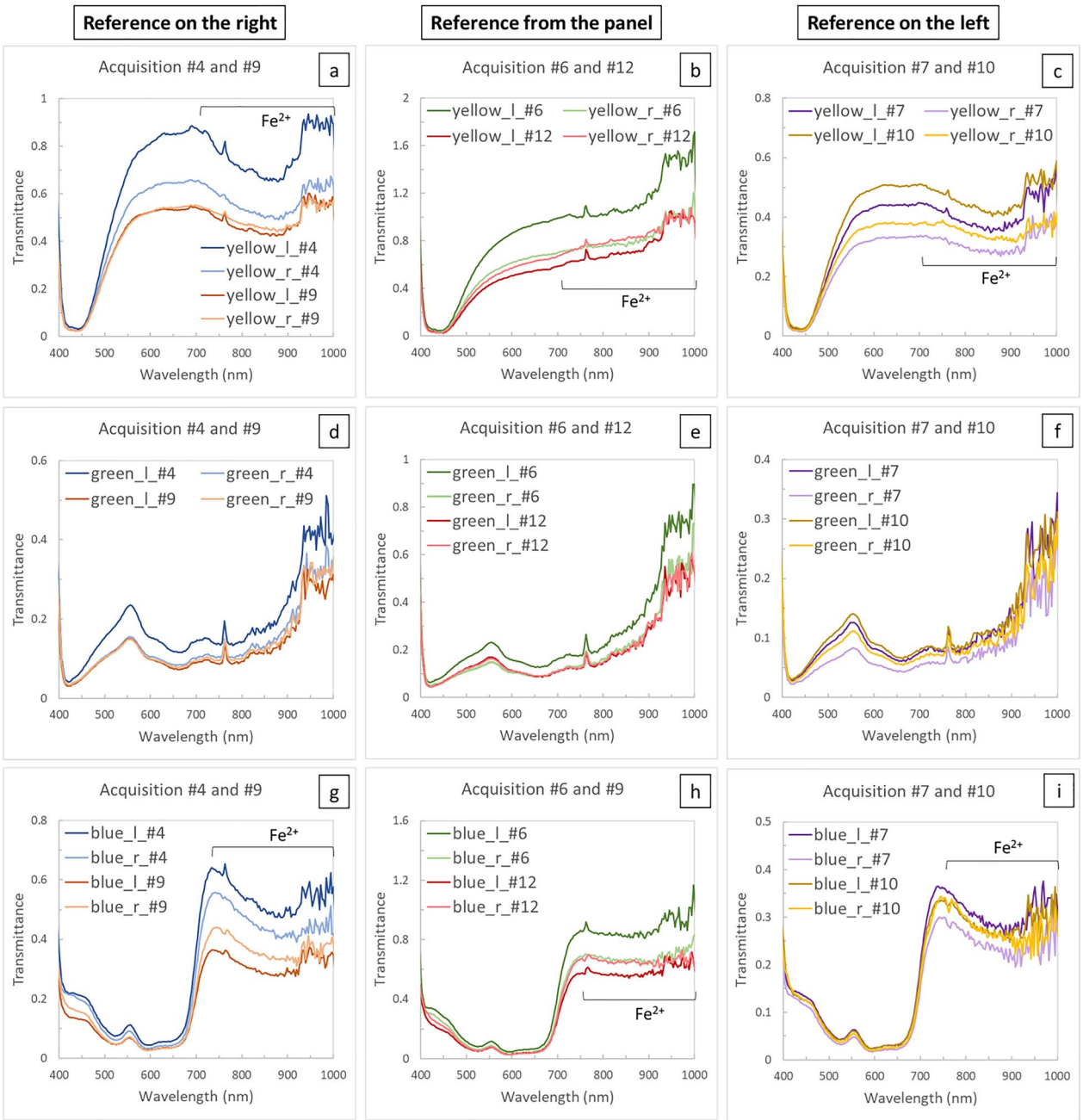

Fig. 9 Comparison of spectra obtained on the left and right side from the pair of datacubes processed using the same glass pane as reference for the three selected colors (yellow, green, and blue). The width of the band in the NIR region associated to Fe^{2+} is indicated. The peak at 750 nm is an artifact probably due to the sunlight spectrum or interference from atmosphere. Notice how the band of Fe^{2+} tends to disappear when the radiometric correction is performed using a transparent area inside the stained-glass panel as reference. Figure 6 shows the points where the spectra were taken

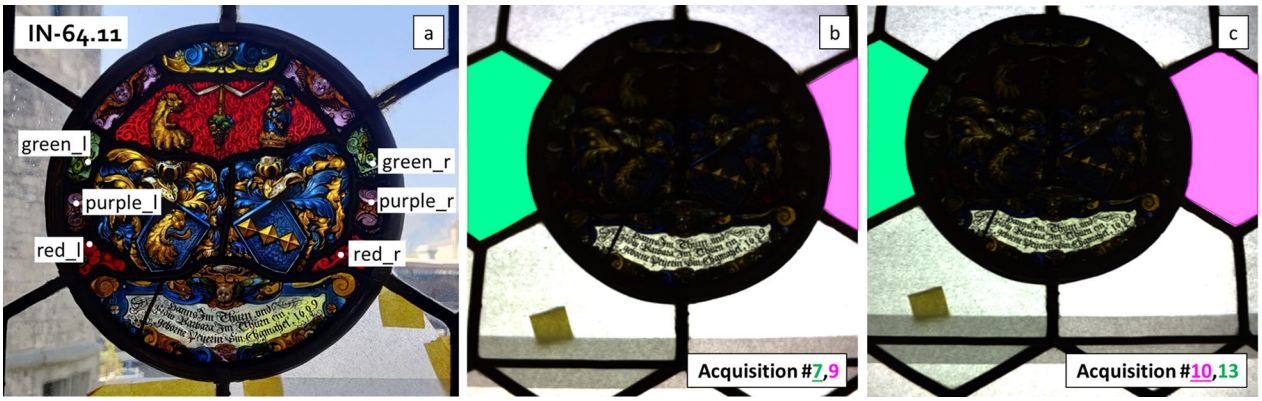

Fig. 10 **a** Close-up picture of case-study IN-64.11, showing the points selected for the spectra comparison. **b** Picture showing the areas chosen as transmittance reference for two of the acquisitions taken in the morning (#7, in green, and #9, in pink). **c** Picture showing the areas chosen as transmittance reference for two of the acquisition taken in the afternoon (#10, in green, and #13, in pink). The underlined number indicates the datacube from which the RGB image was taken

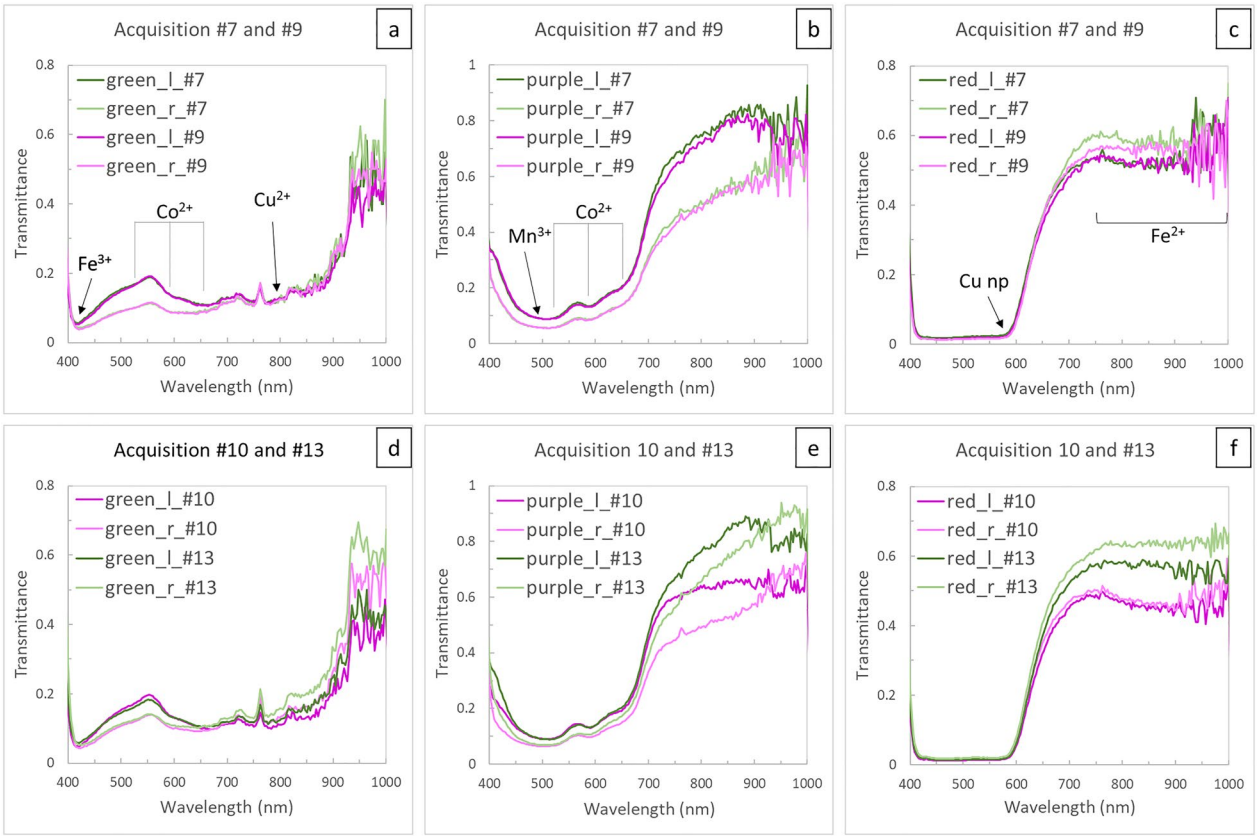

Fig. 11 **a**–**c** Comparison of spectra obtained on the left and right side from the pair of datacubes recorded in the morning, for three selected colors (green, purple, and red). **d**–**f** Comparison of spectra obtained on the left and right side from the pair of datacubes recorded in the afternoon, for the three selected colors (green, purple, and red). The bands' position of the main chromophores (np = nanoparticles) are indicated with arrows, except for Fe^{2+}. Since the maximum of the Fe^{2+} band falls outside the camera spectral range (1100 nm), and the NIR region is quite noisy, it was preferred to indicate the band width for this chromophore. The small peak at 750 nm in **a** and **d** is an artifact probably due to the sunlight spectrum or interference from atmosphere. Postfixs in curve labelling: l = left; r = right. Figure 10 shows the points where the spectra were taken

than those taken from the left side, except for the red-colored glass. It is also worthy of mention that the spectra in the two groups seem to overlap almost perfectly regardless of where the transmittance reference region was selected.

On the other hand, the spectra from the datacubes collected in the afternoon (#10 and #13) show an opposite trend. In this case, the spectra taken from the two sides of the same image are more similar in intensity and shape. At the same time, a difference in the NIR region can be observed between the two datacubes, especially in the red and purple glass. These variations may be explained as follows:

- Morning acquisitions: the stained glass does not receive any direct light in the morning, and the window is open towards the inside from right to left. Thus, the spectral differences may depend on the fact that the left side is less exposed to the light, resulting in spectra with lower intensity.
- Afternoon acquisition: in this case, the sunlight hit from the right side almost directly on the stained glass. This situation probably reduced the variations related to the differences in sunlight exposure of the two sides and enhanced those associated with the selection of the glass pane for transmittance reference. As for the case study AG-1177, a slight difference in the red—NIR region (750–1100 nm) can be noticed, whether the radiometric correction has been performed using a glass panel or another reference. This aspect will be commented on further in "Discussion" section by comparing the results from other case studies presenting a similar situation.

Stained glass within crown-glass windows As mentioned at the beginning of the section, the HSI of stained-glass panels within a crown glass window (Fig. 12) represents a more challenging task than those in widows made of hexagonal panels. The case study LM-8368 was chosen as a representative example to show the consequences of this scenario. The panel is oriented North/East and does not receive direct sunlight at any time of the day. It also faces an urban green area, and many trees are visible in the background, even after applying the diffusing sheet. The strong impact of the vegetation signal is demonstrated by visualizing the false color image of the panel (Fig. 12b, d, f). The false-color image was created with the Fiji software by selecting three images from the datacube corresponding to the green (549 nm), the red (643 nm), and the NIR (811 nm) bands. Those single images were rearranged into a new RGB image, putting the infrared image first, then the red and the green. The result is an image that enhances the difference between similar colors but with different spectral features [21, 22]. In this case, for example, three different situations can be observed depending on which transparent area has been used to perform the radiometric calibration.

The bright pink color visible in most of the transparent areas of the window not covered by the diffuser can be correlated to the vegetation signal, as the images selected for the blue and the green bands fall in regions where the characteristic bands of leaf pigments can be observed (Fig. 13) [23, 24]. The pink color, in different tones, can also be observed in the transparent areas covered by the diffuser in acquisitions #1 and #2, while it is almost absent in acquisition #3. Spectral variations presented in Fig. 13 show the change in intensity of the transmittance band, starting at 700 nm. This is more or less proportional to the intensity of the leaf pigments' bands (500–700 nm) in acquisitions #1 and #2. In acquisition #3, on the other hand, the band's intensity is reduced, but the signal of the leaf pigments is still relatively high. The lower intensity of the band in the NIR might be the reason for the bluish color. This difference in the false color appearance may be correlated to the fact that the three areas where the reference has been taken show a variable amount of vegetation. It might be possible that the signal of vegetation (or the lack of it, as in the case of acquisition #1—see Figs. 12a and 14a) has impacted the radiometric correction in different ways.

The disadvantage of using a tiny area for the radiometric calibration, with such an inhomogeneous background, is well demonstrated by looking at the spectra of red and yellow colored glass. It can be observed from Fig. 14 that the shape of these spectra is distorted depending on the position of the reference glass in relation to the colored glass. Practically, if the reference glass is selected from the upper part of the window (Fig. 14, turquoise area), all the spectra taken from that part until half of the stained glass appear perfectly smooth. On the other hand, the spectra taken from different locations will show an absorbance band starting abruptly at around 700 nm, which may be related to the signal of the vegetation present in the lower part of the stained glass (Fig. 14b, c). The same reasoning can be done if the reference is selected from the lower portion of the window; in this case, the vegetation signal will appear as a bump starting at around 700 nm (Fig. 14d, e). In both cases, these distortions are generated because the area selected as a reference is too small to be considered representative, especially when two highly different areas are in the background. In this case, performing two distinct acquisitions is a good solution to obtain the best results for both halves of the stained glass.

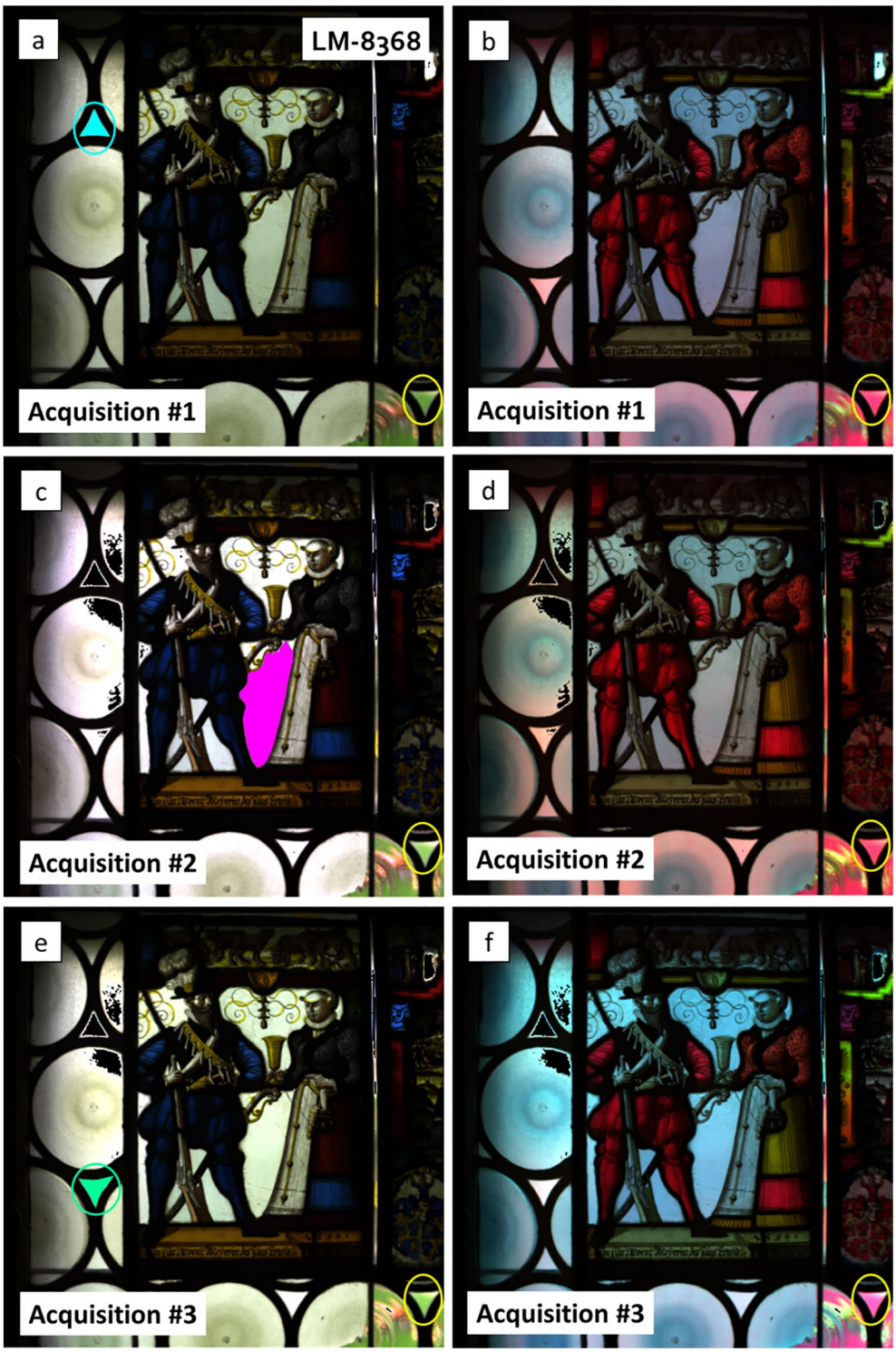

Fig. 12 **a**, **c**, **e** RGB images created by the camera after the acquisition, showing the area where the reference was collected (turquoise triangle for acquisition #1, magenta area for acquisition #2 and green triangle for acquisition #3); **b**, **d**, **f** false color images for each of the acquisitions. The band used to create the false color are stated in Fig. 13. The yellow circle indicates the area where the signal of vegetation (see Fig. 13) was taken. The black pixels visible in the small triangular glass pane and partially in the crown glass on the top left are saturated pixels

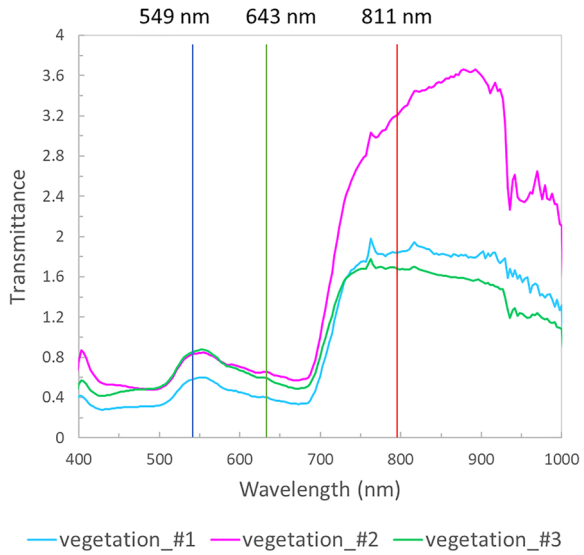

Fig. 13 Spectra of vegetation taken from the small triangle on the bottom-left corner (yellow circle) in Fig. 12. The three lines indicate the wavelengths related to the images selected to reconstruct the false-color image, while the colors of the lines indicate which RGB channel each image substitutes

Internal wall

One of the most significant advantages of analyzing panels within a window of an internal wall is the possibility of using a stable light source instead of solar radiation. This way, the issues related to light variation and noise from the atmosphere signal could be eliminated; however, developing a proper setup to diffuse the light can still be challenging.

As shown in Fig. 2, the lighting setup used in this work consisted of a single halogen studio light positioned in the center of the object under study. The light is diffused by a diffusing textile material commonly used in photography studios, held by a makeshift stretcher and two poles. The studio light and the diffusing fabric were placed at a long distance from each other and from the object to improve the light distribution across the field of view (Fig. 2). However, this was not sufficient to obtain a perfectly diffused illumination. It can be observed from Fig. 15 that the light distribution is characterized by an intensely illuminated area that gradually loses intensity at the edges. The difficulties in keeping the diffusing textile well stretched also contributed to the sub-optimal lighting conditions. The folds generated by the lack of rigidity of the fabric contributed to generating additional shadows within the field of view.

Figure 16 shows the comparison between acquisitions #7 and #6. Acquisition #7 was performed by using a glass pane from the right, and acquisition #6 by using a transparent glass piece inside the stained glass. It can

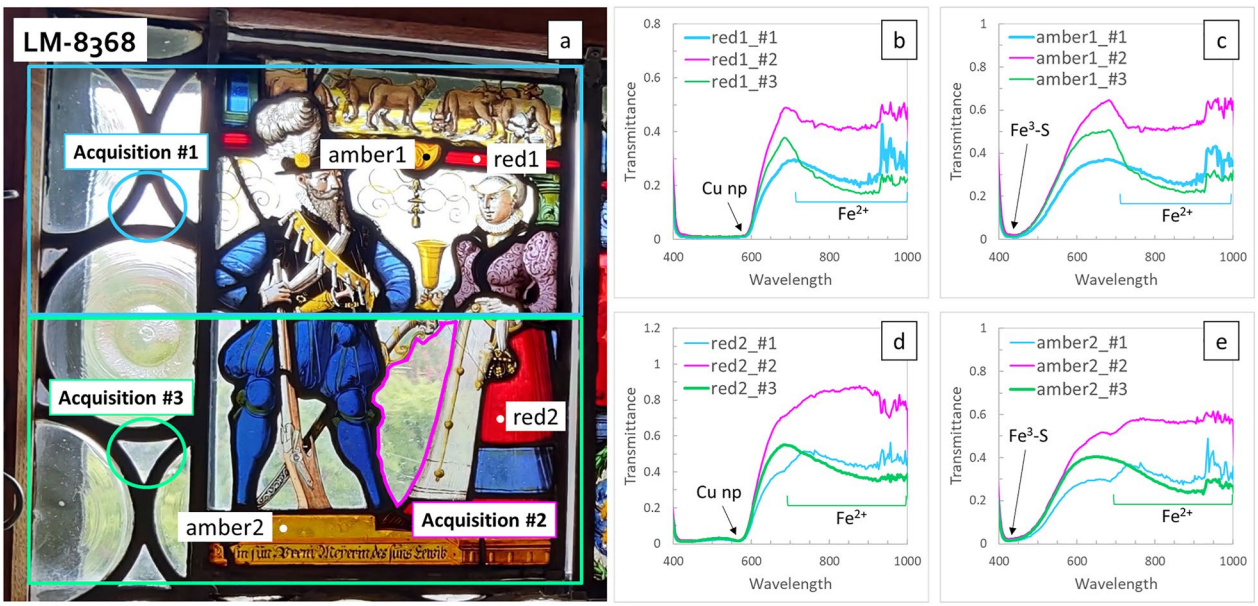

Fig. 14 **a** Close-up picture of case study LM-8368. The green and blue triangle and the magenta border indicates where the references were taken for the three acquisitions. The blue and green rectangular areas delimits the area where the associated reference performs well. **b**–**e** Spectra comparison for amber and red colored glass from three acquisitions performed using three different transparent areas as reference. The bands' position of the Cu nanoparticles (np) and the Fe^{3+}-S complex are indicated with arrows. Regarding Fe^{2+}, it was preferred to indicate the band width for this chromophore, since the maximum of its band falls outside the camera spectral range (1100 nm), and the red-NIR region is distorted by noise and artifacts from the radiometric correction

Fig. 15 **a** Close-up picture of case-study LM-749, showing the points selected for the spectra comparison. **b**, **c** Pictures showing the areas chosen as transmittance reference (in green)

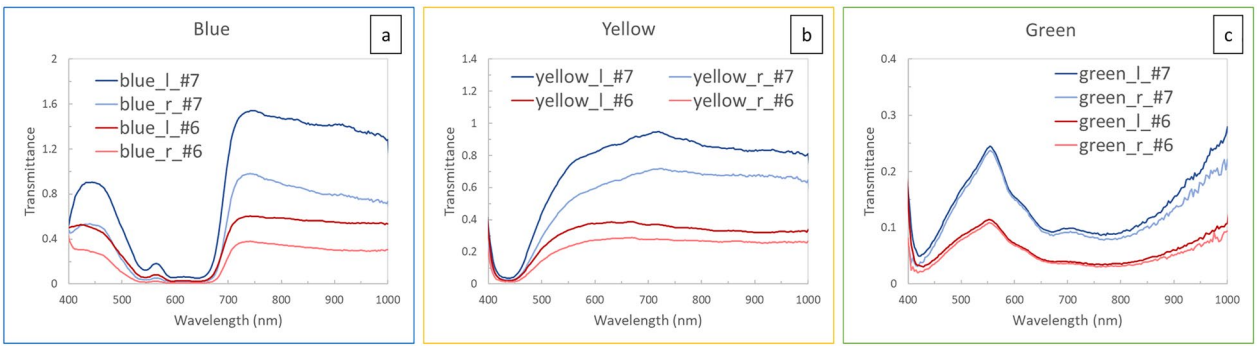

Fig. 16 Comparison of spectra obtained on the left and right side from acquisitions #7 and #6 for three selected colors (blue, yellow, and green). Figure 14 shows the points where the spectra were taken

be noticed that the spectra from acquisition #6 are flatter and smoother in the region after 700 nm, a situation similar to the case study AG-1177. The explanation behind this phenomenon will be discussed in detail in the following section.

Discussion

Importance of reference selection: considerations on chemical composition and background influence

As mentioned in "Results" section, in some case studies (AG-1177, IN-64.11, and LM-749), the spectra present a different shape, whether the radiometric correction is performed using a transparent glass from the stained glass or one of the window panes as reference. Two specific variations can be observed: in the first scenario, such as in the case of AG-1177, the large absorbance band in the NIR region, usually associated with ferrous iron (Fe^{2+}), disappears (Fig. 17, green and red lines) when the transmittance reference is chosen from inside the stained glass. This phenomenon is especially visible in yellow and blue glass (Fig. 17b, c).

By observing the spectra obtained from the datacubes corrected with one of the window's panes (Fig. 17a, blue, orange, gray, and yellow line), the transparent glass of the stained glass likely contains a certain amount of iron as well. Unfortunately, it was impossible to perform XRF analysis on the transparent section of the stained glass, as the area was too small to fit the head of the instrument. However, the spectra seem comparable with results published in the literature regarding the analysis of historical windows [20, 25].

From these considerations, it is possible to hypothesize that, during the image processing, the Fe^{2+} bands are subtracted from the rest of the colored glass, disappearing. If Fe^{2+} is not present in the colored glass in the first place, the distortion appears as an increase of the signal in the NIR region, as shown in the example of the green glass (Fig. 17d).

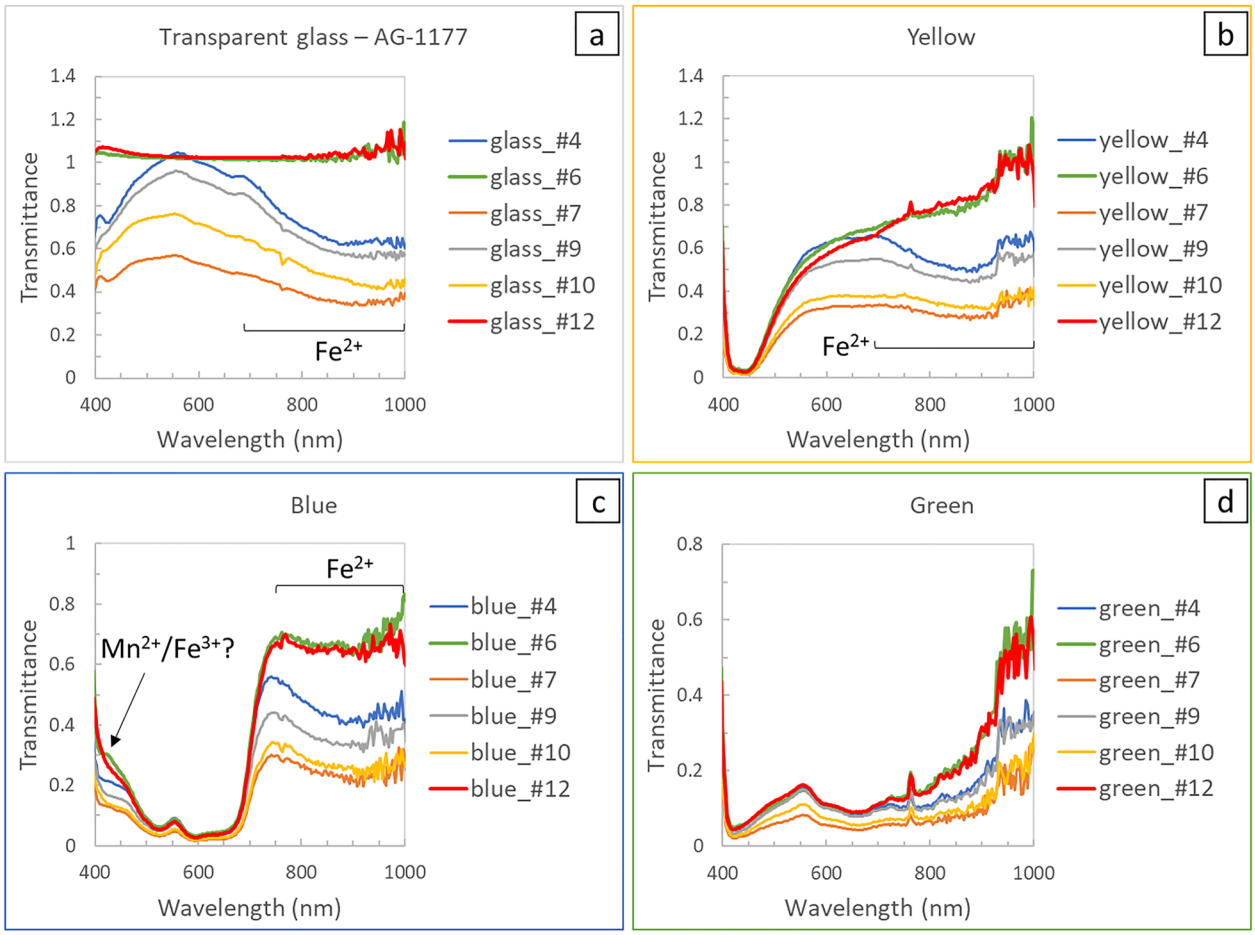

Fig. 17 **a** Comparison of spectra of the transparent area inside the stained glass, taken from all the acquisitions of AG-1177. Each spectrum is an average signal obtained by selecting the entire transparent area (Fig. 8b and e). The red and green lines refer to the spectra obtained when the transmittance reference is taken inside the stained glass, which appear flat due to the division occurring during the image processing phase. The characteristic bands of the transparent glass can be observed when the reference is taken from the windows' panes. **b**–**d** Comparison of spectra of yellow, blue, and green glass on the right side of the panel, taken from all the acquisitions. The red and green lines refer to the spectra obtained when the transmittance reference is taken inside the stained glass and appear slightly different from the others due to effects related to the radiometric correction. Figure 6 shows the points where the spectra of colored glass were taken

The same phenomenon has also been partially observed in the case study IN-64.11, especially in red and purple glass (Fig. 11e and f). In the case of purple glass, as for the green glass, the distortion appears as a signal increase in the NIR region. Unlike the other examples, however, this panel has no original transparent area sufficiently large to be used as a reference. It is worth reminding that the windows where the panels are placed were produced with historical recipes and are not as pure as contemporary glass would be. In addition, the various glass panes composing the windows may have been substituted through time for reparation before being installed in the museum or even afterward. In this case, qualitative XRF analysis (see Additional file 2, Fig. s5) revealed that the hexagonal glass panes on the right side contain a lower amount of iron and manganese than the one on the left side, which may explain this difference.

In the second scenario, the spectra of stained-yellow glass from datacubes processed using a glass pane from the historical window show three additional bands (at around 530, 590, and 660–680 nm). This behavior can be observed in two very different situations: in the first case (LM-8368), vegetation is present in the background; at first look, these additional bands may be related to the signal of the vegetation in the background of the stained glass (Fig. 18a, b), which signal should have been limited by the diffusing sheet. A strong transmittance band starting abruptly at around 700 nm can also be observed.

In the second case (LM-749), when vegetation is absent, the reason behind the additional bands (at around

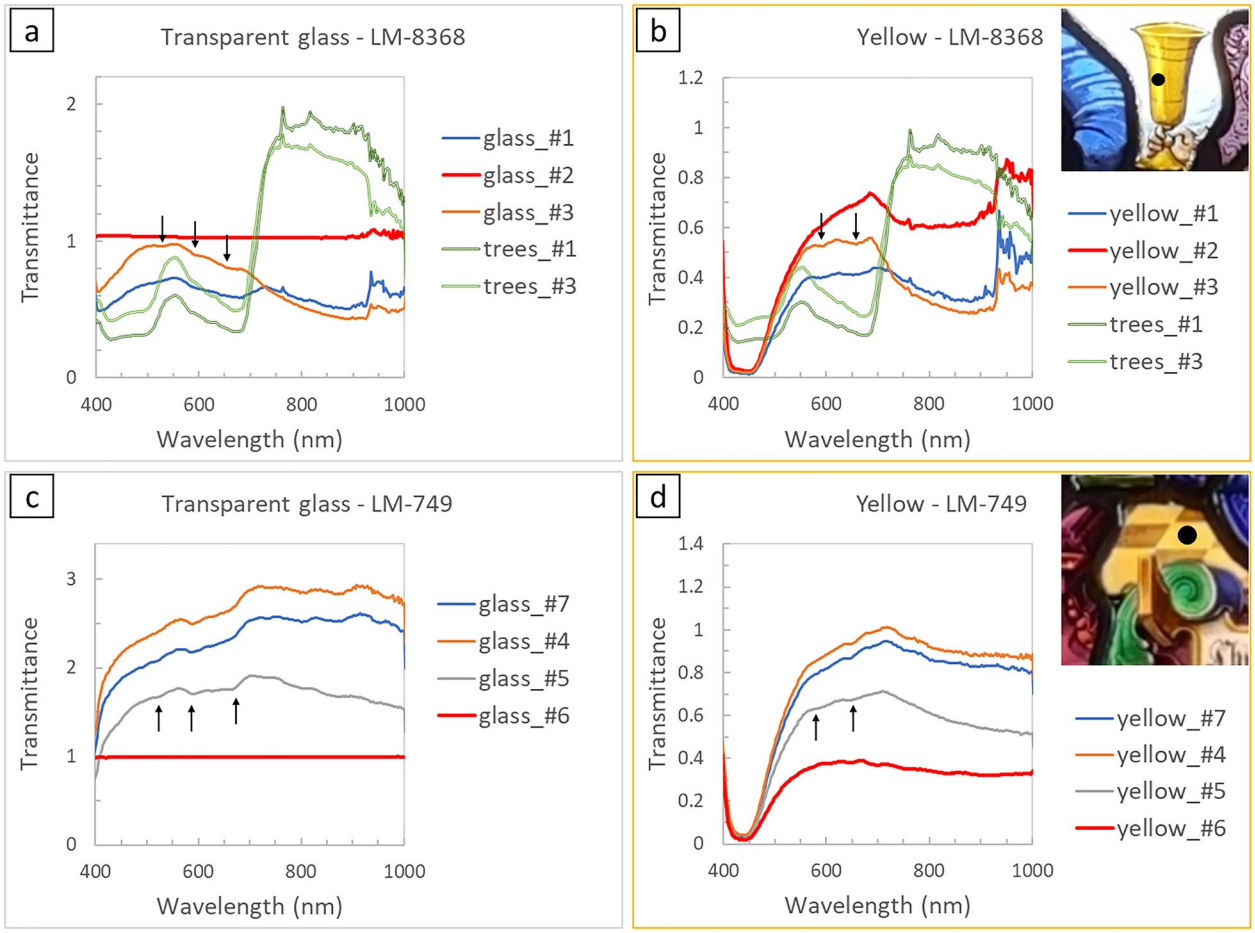

Fig. 18 **a** Comparison between spectra from the transparent area inside the stained glass and the vegetation. The spectra are taken from all the acquisitions of LM-8368. Each spectrum is an average signal obtained by selecting the entire transparent area (Fig. 14a). The red line refers to the spectra obtained when the transmittance reference is taken inside the stained glass, which appears flat due to the division occurring during the image processing phase. The characteristic bands of the transparent glass can be observed when the reference is taken from the windows' panes. **b** Comparison between spectra of an area painted with stained yellow and vegetation, taken from all the acquisitions of LM-8368. The red line refers to the spectra obtained when the transmittance reference is taken inside the stained glass and appears slightly different from the others due to effects related to the radiometric correction. **c** Comparison of spectra of the transparent area inside the stained glass (Fig. 15c), taken from all the acquisitions of LM-749. **d** Comparison between spectra from an area painted with stained yellow, taken from all the acquisitions of LM-749

530–540, 590–600, and 660 nm) may be associated with cobalt (Co^{2+}) impurities. The fact that these bands are also visible in the yellow-colored glass may be related to the thinness of the stained yellow layer. The similarity of the spectral shapes in the two scenarios depends on the fact that the leaf pigments and the cobalt ions absorb light almost in the same region [20, 23–25]. However, when radiometric calibration is performed using the transparent area inside the stained glass, the three bands tend to disappear entirely in both cases (red lines, Fig. 18b, d). For this reason, in the case of LM-8368, those bands cannot be related to vegetation but most probably to the composition of the transparent glass used as reference. Following the same reasoning formulated previously regarding Fe^{2+}, it might be possible that the three bands of Co^{2+} are eliminated during the image processing phase. This means that even when vegetation is present, it is still possible to infer the presence of cobalt impurities if a diffusing sheet is applied.

XRF analysis was performed on the transparent area of LM-8368 to characterize the glass composition and verify this hypothesis. However, it was not possible to detect cobalt in the glass, as its concentration was probably under the instrument's detection limit.

Between the two situations, a slight difference can still be observed: if vegetation is present in the background, the strong absorbance band between 700 and 1000 nm is still visible, even if the reference is selected from a

transparent area inside the stained glass (Fig. 18b, red line). This fact means that, in the presence of vegetation, the selection of the transmitting reference inside or outside the stained-glass panel does not entirely eliminate the influence of the background from the final results.

In light of these considerations, it is clear that the transmittance reference selection can significantly impact the quality of the results. Repeating the acquisition multiple times using different transparent areas as a reference, together with a good knowledge of the fingerprint absorbance bands of the main chromophores, can help identify any anomalies in the results obtained and avoid erroneous interpretation.

Effectiveness of in-situ hyperspectral imaging for chromophore identification

Despite the numerous challenges discussed in the previous sections, in-situ HSI can still represent a valuable tool for the preliminary characterization of chromophores in stained glass. In light of the results obtained from the case studies, it is possible to draw some conclusions about the effectiveness of the in-situ application of hyperspectral imaging.

In general, the spectral range between 450 and 700 nm is not affected by the background unless vegetation is present. Nonetheless, using a diffusing sheet can help eliminate the vegetation's signal, as shown in the case of AG-1177. The following bands are almost always recognizable, regardless of the reference selection:

- The surface plasmonic resonance (SPR) of the copper nanoparticles in red glass (Cu^0) at around 565 nm (Figs. 11c, f, 14b, d) [12, 13, 26, 27].
- The broad band of Mn^{3+} in purple glass, at about 490–500 nm (Fig. 11b, e) [12, 13, 26, 28].
- The three bands of Co^{2+} in blue (Figs. 7l, 9g–i, 16a), green (Figs. 7k, 9d–f, 11a, d, 16c), and purple glass (Fig. 11b, e), at around 530–540, 590–600, and 650–670 nm [12, 13, 26, 27]. However, the band at about 590–600 nm may disappear if the glass used as a reference contains cobalt impurities (Fig. 16a).
- The band associated with silver nanoparticles (Ag^0) in glass painted with stained yellow (Figs. 7j, 9a–c, 16b). The position of this band may vary between 420 and 450 nm. The shift is usually influenced by the dimension and shape of the silver nanoparticles, as well as the possible presence of copper nanoparticles and the proportions in the Ag–Cu mixture. [29–31].
- The band associated with the ferric-sulfide (Fe^{3+}-S) complex in amber glass at around 410–420 nm (Fig. 14c, e) [26, 27].

On the other hand, the characteristic bands of Fe^{2+}, Fe^{3+}, Mn^{2+}, and partially Cu^{2+} are more prone to be altered for the following reasons:

- The intensity of the Fe^{2+} band is very susceptible to the amount of this oxide contained in the transparent glass used as a reference.
- The Fe^{3+}, Mn^{2+}, and the iron-manganese complex absorption bands, located at the end of the camera's spectral range in the UV region [19, 20, 28], can be masked or altered by a noise peak present in almost all the spectrum at around 400 nm, more or less intense depending on the imaging conditions.
- The region between 650 and 1000 nm is generally noisier on green glass pieces (probably due to their dark color and low transmittance), resulting in alterations of the absorbance band of Cu^{2+}, located at around 780–800 nm [12, 26, 27].
- If the acquisition is performed using sunlight as the light source, part of the Fe^{2+} and Cu^{2+} bands in the NIR region can be altered by the noise generated by the atmospheric water.

The alterations described above can considerably impact the data interpretation, especially when they hinder the identification of iron oxides (Fe^{3+} and Fe^{2+}) and manganese (as Mn^{2+}) since they can be used to determine the provenance of raw materials, furnace conditions, and the age of the glass under study [20]. The general color appearance of the stained glass can also be affected. For example, in Fig. 8, it is possible to notice that when the reference is selected from within the panel, the glass pieces appear less yellow. It is possible that the slight coloration of the transparent glass, given by iron impurities or wanted addition, is eliminated during the image processing step. In this case, repeating the measurements using different transparent glass sections can help verify any change in the spectral shape of both colored and uncolored glass and identify eventual anomalies.

In the previous sections, the identified chromophores were briefly indicated in the plots of all the studied panels. Here, on the other hand, the case studies LM-749 and LM-660.1 (Figs. 19 and 20) are shown as examples to highlight the potential of HSI in distinguishing glass of similar colors made with different chromophores. LM-749, as stated in section "Internal wall", has been acquired using a stable light source and homogeneous background. On the other hand, LM-660.1, as LM-8368, is located within a crown glass window facing an urban green space with trees. Despite the two different situations, it was possible to successfully identify the main chromophores for both stained glass (Figs. 19 and 20).

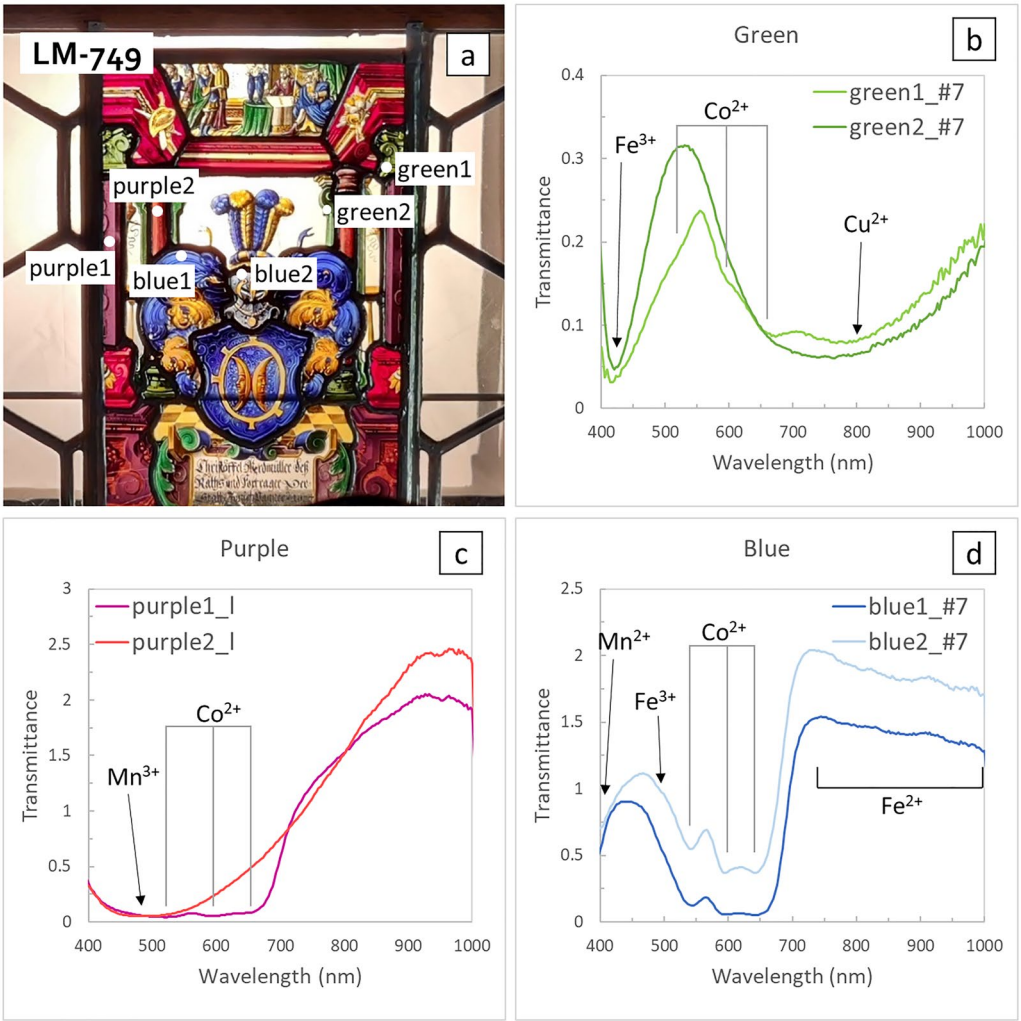

Fig. 19 **a** Close-up picture of case-study LM-794, showing the points selected for the spectra comparison. **b** Comparison of two green glass. **c** Comparison of two purple glass; **d** Comparison of two blue glass. The bands' position of the main chromophores are indicated

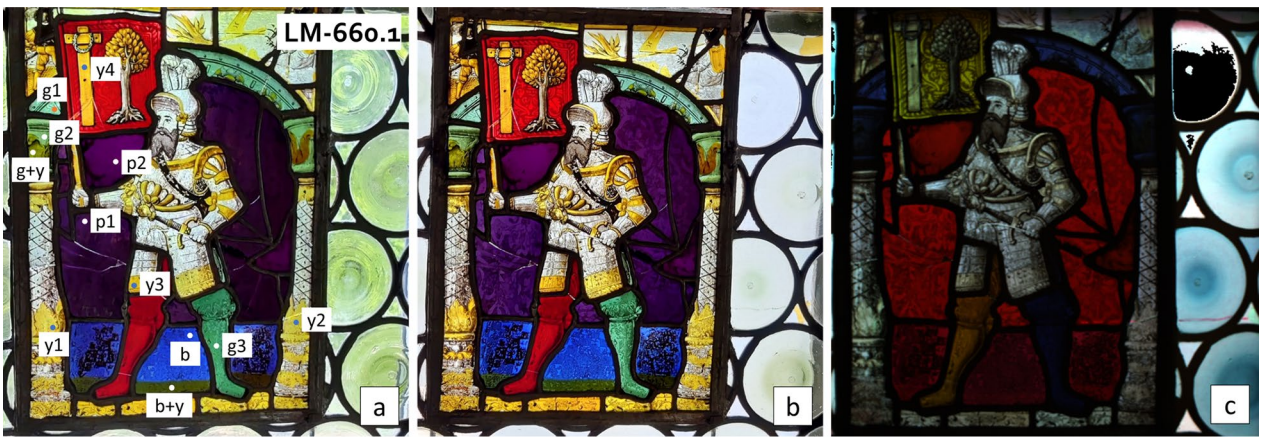

Fig. 20 **a** Close-up picture of case-study LM-660.1, showing the points selected for the spectra comparison. **b** Close-up picture of case-study LM-660.1, after the application of the diffusing sheet. **c** False-color image obtained from acquisition #6

In LM-749, for example, it is possible to identify two types of green and purple glass (Fig. 19). Regarding the green glass, the darker one was obtained using only Cu^{2+} (the broad band with an absorbance maximum at 780 nm), and Fe^{3+} (band at around 420 nm), while the lighter green shows the addition of Co^{2+} (three bands at 540, 590, and 660 nm). Concerning the purple glass, the reddish-purple one seems to contain only Mn^{3+} as the main chromophore (490 nm), while the other purple glass has a more bluish hue due to the additional presence of Co^{2+}.

On the other hand, the pale and the darker blue seem to have been colored using the same chromophores (mainly cobalt) but in different concentrations. The slight difference in the region between 450 and 500 nm could be related to a different amount of Fe^{3+} in the two areas (additional weak band at 480–490 nm)[19], but further analyses should be performed to confirm this hypothesis.

The case study LM-660.1 (Fig. 20) is particularly interesting from the conservation-restoration point of view. For instance, a few purple glass pieces have probably been

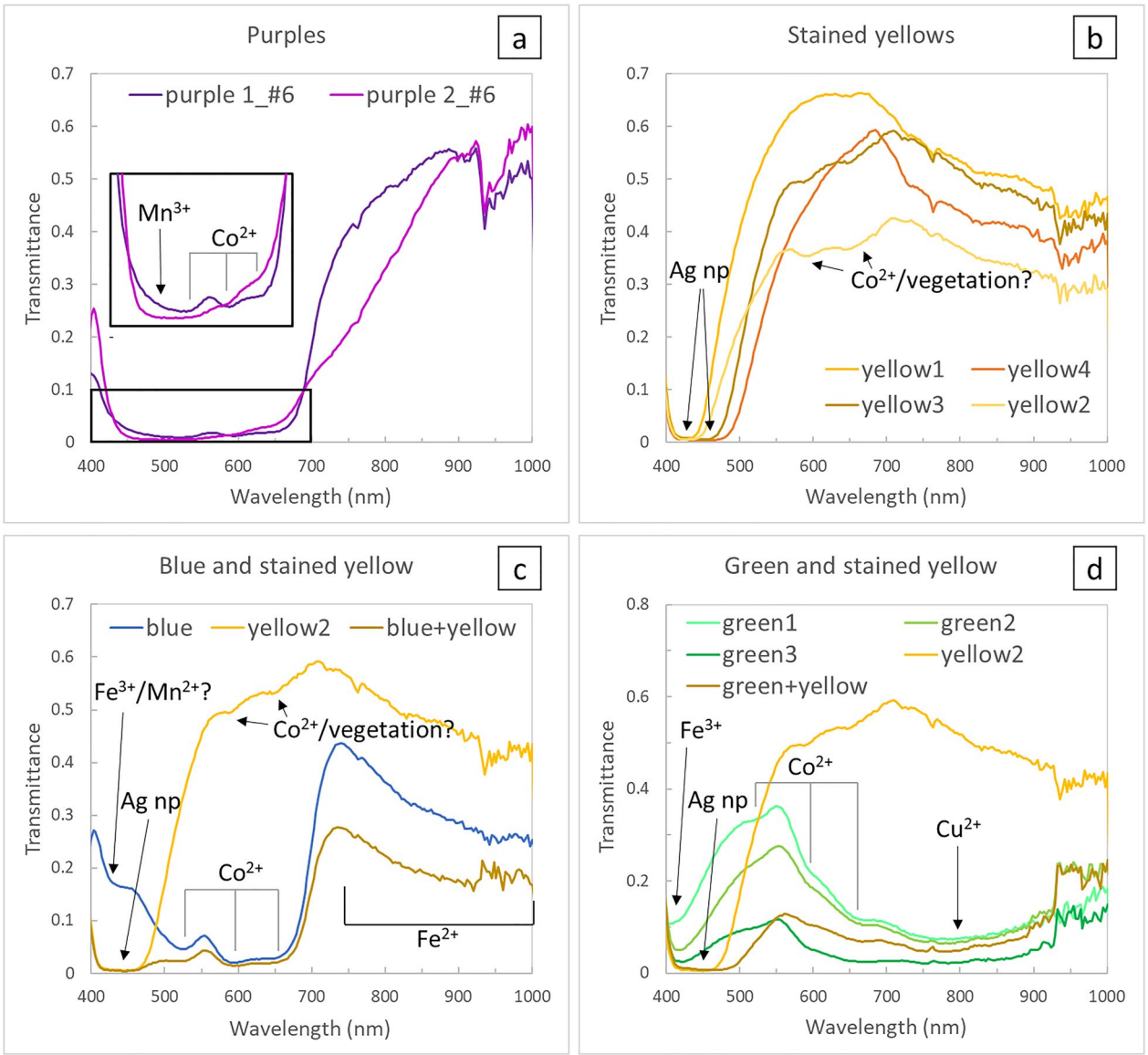

Fig. 21 **a** Comparison of the original purple glass with a probable later addition. **b** Comparison of four stained yellows, characterized by a shift of the silver nanoparticles band from 420 (light yellow) to 450 nm (intense yellow); **c** Comparison of blue glass, stained yellow and the combined layers. **d** Comparison of green glass, stained yellow and the combined layers. The band's position of the main chromophores are indicated. Figure 20a shows the points where the spectra were taken

substituted using purple glass with a different composition. This theory seems to be confirmed by comparing the spectra from the original purple glass and the possible addition (Fig. 21a), which shows how the replacement glass contains a lower amount of cobalt.

Thanks to HSI, it was also possible to understand the application of the stained yellow layer across the stained-glass panel. Figure 21b shows the spectra of possibly four typologies of stained yellow, characterized by a shift of the silver nanoparticle band from 420 (light yellow) to 450 nm (intense yellow). According to the literature, this shift may be related to the size and dimension of the silver nanoparticles or the addition of copper nanoparticles, which provided an orange color to the stained yellow [29–31].

Stained yellow has also been applied over blue and green glass to depict details like the capitals' decorations and the pavement's border. Figure 21c and d show how it is possible to distinguish the contributions of the two layers by comparing the spectrum of the mixed layer with those of the pure colors. The spectra of the blue and green glass, covered by stained yellow, are both characterized by the painted layer's contribution in the region between 420 and 460 nm, while the rest of the spectrum shows the characteristic bands of the chromophores of the layer below. This is especially noticeable in the blue glass (Fig. 21c).

Conclusion

This paper presented the results from an extensive *in-situ* hyperspectral imaging campaign on stained glass windows exhibited at the Swiss National Museum. Hyperspectral imaging was applied both on stained glass exposed to sunlight and on stained glass displayed in a window of an inner wall to evaluate the challenges related to these two different environments and identify the advantages and limitations of the technique.

Regarding stained glass exposed to sunlight, the results' quality depends significantly on the size and chemical composition of the transparent area chosen as reference and external factors such as the presence of vegetation and changing illumination throughout the day. In this specific case, the possibility of applying a diffusing sheet behind the panels allowed for minimizing the influence of these external factors and obtaining successful results in most cases. However, the authors are aware of this situation's exceptionality and that it may not always be possible to apply this methodology everywhere (for example, in large windows of religious or secular buildings that cannot be opened). It is also worth mentioning that the collaboration with the museum's staff and conservators was essential to test this approach to ensure that opening the window and applying the diffusing sheet was not damaging the artworks.

Factors such as the weather, and the sun's position in relation to the object during the acquisitions, must also be taken into consideration since they determine the amount of light reaching the stained glass and its distribution. During the preliminary tests and the imaging *in-situ*, it has been observed that a foggy day or a clear sky (with the sun far away from the field of view) provides the most homogeneous background and, consequently, the best imaging conditions. On the other hand, the light intensity may be too low to allow the identification of the darkest-colored glass, especially the green ones. In this case, having direct sunlight in the field of view can improve the visualization of the deep-colored glass. However, the contrast between the more illuminated areas with the rest of the scene can become an issue during the radiometric correction. The risk of overexposing the light-colored glass is also very high due to the intensity of the solar radiation reaching the stained glass, even with a minimal camera exposure time. The best moment for the acquisition should then be judged case-by-case, making compromises according to the research questions that need to be answered. If budget and time allow, it would be advisable to perform multiple acquisitions, not only on the same day but also in different seasons and weather conditions.

Concerning the panels displayed on internal walls' windows, a lighting setup was developed to perform the HSI acquisition. The makeshift system allowed encouraging results; however, it still necessitates improvements. In this sense, further work should be focused on implementing a rigid diffuser to avoid the formation of rippling shadows due to the folds of the fabric. Using multiple light sources instead of a single one is advised to improve light distribution.

In both situations, nonetheless, it was possible to acquire sufficiently good results to have a qualitative understanding of the chromophores involved in the coloration of the glass pieces in a completely non-invasive way. While some characteristic bands could be altered due to external or camera-related issues, a good knowledge of the absorption behavior of chromophores can help formulate initial hypotheses, which can then be validated by complementary analysis.

Supplementary Information

The online version contains supplementary material available at https://doi.org/10.1186/s40494-023-00923-6.

Additional file 1: Table s1. Acquisitions parameters of case study IN-11.64. **Table s2.** Acquisitions parameters of case study AG-1177. **Table s3.** Acquisitions parameters of case study LM-8368. **Table s4.** Acquisitions parameters for case study LM-749. **Table s5.** Acquisition

parameters for case study LM-749. **Figure s1**. sun position during HSI acquisitions for case study AG-1177, calculated through the website SunCalc.org. **Figure s2**. Sun position during HSI acquisitions for case study IN-64.11, calculated through the website SunCalc.org. **Figure s3.** sun position during HSI acquisitions for case study LM-8368, calculated through the website SunCalc.org.

Additional file 2: Figure s4. a) close-up picture of case-study AG-1177, showing the point selected for the XRF analyisis. b) XRF spectra of the two glass panes used as reference for radiometric correction. c) zoom of the spectra showing the differences in concentration of iron and manganese in the two glass panes. **Figure s5.** a) close-up picture of case-study LM-8368, showing the point selected for the XRF analyisis. b) XRF spectra of the two glass panes used as reference for radiometric correction. c) zoom of the spectra showing the differences in concentration of iron and manganese in the two glass panes.

Additional file 3: Table s6. Technical information and number of acquisitions taken for the case studies LM-2632.c and AG-1183. **Table s7.** Acquisitions parameters of case study LM-2632. **Table s8.** Acquisitions parameters of case study AG-1183. **Figure s6.** a) close-up picture of case-study LM-2632.c, showing the points selected for the spectra comparison. b) pictures showing the areas chosen as transmittance reference (in green). c) spectra comparison of two purple glass. d) spectra comparison of two blue glass, one light and one dark. The dark blue is enamel glass charachterized by areas with different thickness. Notice how the band of Co^{2+} at 590 nm disappears in thicker areas. e) spectra comparison of two green glass with different composition. D) Spectra comparison of stained-yellow and amber glass. Stained-yellow glass shows two peaks at around 590–600 and 660 nm which may be related to cobalt impurities from the transparent glass. **Figure s7.** a) close-up picture of case-study AG-1183, showing the points selected for the spectra comparison. b) pictures showing the areas chosen as transmittance reference (in green). c) spectra comparison of two purple glass; one containing cobalt as additional chromophore d) spectra comparison of three blue glass, obtained from different concentration of iron and cobalt. Manganese (as uncolored Mn^{2+}) may be present in higher concentration in the lighter glass. e) spectra comparison of three flashed red glass. The different position and shape of the band at 565 nm could be related to variations in size and dimension of the copper nanoparticles (np). d) Spectra comparison of stained-yellow and amber glass. Besides visual examination, from the spectral point of view the two colored glass can be distinguished from the shape of the slope in the region between 400–550.

Acknowledgements
The authors would like to thank Tino Zagermann, conservator-restorer, for his help during the acquisitions at the Swiss National Museum and Dr. Mylène Rouss, curator at the SNM, for the permission to analyze the stained-glass windows.

Author contributions
Conceptualization, AB, TL, KS, SG, and JYH; methodology, AB; resources, AB, TL, KS; investigation (HSI), AB, TL (supporting); investigation (XRF), TL; formal analysis, AB; visualization, AB; writing—original draft preparation, AB; writing—review and editing, AB, TL, KS, SG, and JYH; supervision, TL, KS, SG, and JYH; project administration, SG, JYH; funding acquisition, JYH. All authors read and approved the final manuscript.

Funding
Open access funding provided by Norwegian University of Science and Technology. This research has been carried out as part of a PhD program within the CHANGE Innovative Training Network. The CHANGE-ITN project has received funding from the European Union's Horizon 2020 research and innovation program under the Marie Skłodowska-Curie grant agreement No. 813789.

Availability of data and materials
The most relevant data generated or analyzed during this study are included in this published article (and its supplementary information files). Additional datasets used and analyzed during the current study are available from the corresponding author upon reasonable request.

Declarations

Competing interests
The authors declare that they have no competing interests.

Received: 28 December 2022 Accepted: 2 April 2023
Published online: 14 April 2023

References

1. Picollo M, Cucci C, Casini A, Stefani L. Hyper-spectral imaging technique in the cultural heritage field: new possible scenarios. Sensors (Basel). 2020;20(10):2843.
2. Radpour R, Delaney JK, Kakoulli I. Acquisition of high spectral resolution diffuse reflectance image cubes (350–2500 nm) from archaeological wall paintings and other immovable heritage using a field-deployable spatial scanning reflectance spectrometry hyperspectral system. Sensors. 2022;22(5):1915.
3. Cutajar JD, Babini A, Deborah H, Hardeberg JY, Joseph E, Frøysaker T. Hyperspectral imaging analyses of cleaning tests on Edvard Munch's monumental Aula paintings. Stud Conserv. 2022;67(sup1):59–68.
4. Gabrieli F, Delaney JK, Erdmann RG, Gonzalez V, van Loon A, Smulders P, et al. Reflectance Imaging Spectroscopy (RIS) for operation night watch: challenges and achievements of imaging rembrandt's masterpiece in the glass chamber at the Rijksmuseum. Sensors. 2021;21(20):6855.
5. Cucci C, Picollo M, Chiarantini L, Uda G, Fiori L, De Nigris B, et al. Remote-sensing hyperspectral imaging for applications in archaeological areas: non-invasive investigations on wall paintings and on mural inscriptions in the Pompeii site. Microchem J. 2020;158: 105082.
6. Balas C, Epitropou G, Tsapras A, Hadjinicolaou N. Hyperspectral imaging and spectral classification for pigment identification and mapping in paintings by El Greco and his workshop. Multimedia Tools Appl. 2018;77(8):9737–51.
7. Cucci C, Bracci S, Casini A, Innocenti S, Marcello P, Stefani L, et al. The illuminated manuscript Corale 43 and its attribution to Beato Angelico: non-invasive analysis by FORS, XRF and hyperspectral imaging techniques. Microchem J. 2017;138:45–57.
8. Cucci C, Delaney JK, Picollo M. Reflectance hyperspectral imaging for investigation of works of art: old master paintings and illuminated manuscripts. Acc Chem Res. 2016;49(10):2070–9.
9. Daniel F, Mounier A. Mobile hyperspectral imaging for the non-invasive study of a mural painting in the Belves Castle (France, 15th C). Sci Technol Archaeol Res. 2015;1(2):81–8.
10. Funatomi T, Ogawa T, Tanaka K, Kubo H, Caron G, Mouaddib EM, et al. Eliminating temporal illumination variations in whisk-broom hyperspectral imaging. Int J Comput Vision. 2022;130:1310–24.
11. Perri A, Nogueira de Faria BE, Ferreira DCT, Comelli D, Valentini G, Preda F, et al. Hyperspectral imaging with a TWINS birefringent interferometer. Opt Express. 2019;27(11):15956–67.
12. Palomar T, Grazia C, Cardoso IP, Vilarigues M, Miliani C, Romani A. Analysis of chromophores in stained-glass windows using Visible Hyperspectral Imaging in-situ. Spectrochimica Acta Part a-Mol Biomol Spectrosc. 2019;223: 117378.
13. Rebollo E, Ratti F, Cortelazzo GM, Poletto L, Bertoncello R. New trends in imaging spectroscopy: the non-invasive study of the Scrovegni Chapel stained glass windows. Proc SPIE, O3A: Optics for Arts, Architecture, and Archaeology III. 80842011. p. 808407.
14. Babini A, Green P, George S, Hardeberg JY. Comparison of hyperspectral imaging and fiber-optic reflectance spectroscopy for reflectance and transmittance measurements of colored glass. Heritage. 2022;5(3):1401–18.
15. Babini A, George S, Hardeberg JY. Hyperspectral imaging workflow for the acquisition and analysis of stained-glass panels. Proc SPIE Optics for Arts, Architecture, and Archaeology VIII. 11784 2021. p. 117841F
16. Behmann J, Acebron K, Emin D, Bennertz S, Matsubara S, Thomas S, et al. Specim IQ: evaluation of a new, miniaturized handheld hyperspectral camera and its application for plant phenotyping and disease detection. Sensors. 2018;18(2):441.

17. Picollo M, Casini A, Cucci C, Jussila J, Poggesi M, Stefani L. A New Compact VNIR Hyperspectral Imaging System for Non-Invasive Analysis in the Fine Art and Architecture Fields. Proceedings e report: Firenze University Press; 2018. p. 69–74.
18. Schindelin J, Arganda-Carreras I, Frise E, Kaynig V, Longair M, Pietzsch T, et al. Fiji: an open-source platform for biological-image analysis. Nat Methods. 2012;9(7):676–82.
19. Micheletti F, Orsilli J, Melada J, Gargano M, Ludwig N, Bonizzoni L. The role of IRT in the archaeometric study of ancient glass through XRF and FORS. Microchem J. 2020;153: 104388.
20. Meulebroeck W, Nys K, Patin M, Thienpont H. The interaction between daylight and fifteenth and sixteenth century glass windows from the low countries. Sci Rep. 2021;11(1):21338.
21. Hayem-Ghez A, Ravaud E, Boust C, Bastian G, Menu M, Brodie-Linder N. Characterizing pigments with hyperspectral imaging variable false-color composites. Appl Phys A. 2015;121:939–47.
22. Buoso MC, Ceccato D, Zafiropoulos D. False-color Infra Red Photography in the Identification of Pigments Used for a late 13th Century Illuminated Manuscript. LNL Annual Report, Applied and Interdisciplinary Physics Instrumentation 2009:153–4.
23. Thenkabail P, Mariotto I, Gumma M, Middleton E, Landis D, Huemmrich K. Selection of hyperspectral narrowbands (HNBs) and composition of hyperspectral twoband vegetation indices (HVIs) for biophysical characterization and discrimination of crop types using field reflectance and hyperion/EO-1 Data. IEEE J Sel Top Appl Earth Obs Remote Sensing. 2013;6:427–39.
24. Jiang J, Comar A, Burger P, Bancal P, Weiss M, Baret F. Estimation of leaf traits from reflectance measurements: comparison between methods based on vegetation indices and several versions of the PROSPECT model. Plant Methods. 2018;14(1):23.
25. Cagno S, Van der Snickt G, Legrand S, Caen J, Patin M, Meulebroeck W, et al. Comparison of four mobile, non-invasive diagnostic techniques for differentiating glass types in historical leaded windows: MA-XRF, UV–Vis–NIR. Raman Spectrosc IRT X-Ray Spectrom. 2021;50(4):293–309.
26. Bracci S, Bartolozzi G, Burnam RK, Corallini A. Integration of both non-invasive and micro-invasive techniques for the archaeometric study of the stained-glass window Apparizione degli Angeli in the basilica of Santa Croce in Florence. Italy. J Cult Heritage. 2020;44:307–16.
27. Hunault MOJY, Bauchau F, Boulanger K, Hérold M, Calas G, Lemasson Q, et al. Thirteenth-century stained glass windows of the Sainte-Chapelle in Paris: an insight into medieval glazing work practices. J Archaeol Sci Rep. 2021;35: 102753.
28. Bidegaray A-I, Godet S, Bogaerts M, Cosyns P, Nys K, Terryn H, et al. To be purple or not to be purple? How different production parameters influence colour and redox in manganese containing glass. J Archaeol Sci Rep. 2019;27: 101975.
29. Patin M, Nys K, Thienpont H, Meulebroeck W. Prestige markers in art: subtle stratagems in material selection for fifteenth-century stained-glass windows. Heritage Sci. 2022;10(1):106.
30. Delgado J, Vilarigues M, Ruivo A, Corregidor V, da Silva RC, Alves LC. Characterisation of medieval yellow silver stained glass from Convento de Cristo in Tomar, Portugal. Nucl Instrum Methods Phys Res, Sect B. 2011;269(20):2383–8.
31. Molina G, Murcia S, Molera J, Roldan C, Crespo D, Pradell T. Color and dichroism of silver-stained glasses. J Nanopart Res. 2013;15(9):1932.

Publisher's Note